REMOTE SENSING LETTERS, 2017
VOL. 8, NO. 4, 301–310
http://dx.doi.org/10.1080/2150704X.2016.1264020

Taylor & Francis
Taylor & Francis Group

Evaluation of the Standardized Precipitation Index as an early predictor of seasonal vegetation production anomalies in the Sahel

Michele Meroni[a], Felix Rembold[a], Dominique Fasbender[a] and Anton Vrieling[b]

[a]Directorate D - Sustainable Resources, Food Security Unit, European Commission, Joint Research Centre (JRC), Ispra, VA, Italy; [b]Faculty of Geo-Information Science and Earth Observation (ITC), University of Twente, Enschede, The Netherlands

ABSTRACT

We analysed the performance and timeliness of the Standardized Precipitation Index (SPI) in anticipating deviations from mean seasonal vegetation productivity in the Sahel. Gridded rainfall estimates are used to compute the SPI for 1–6-month timescales, whereas the *Z*-score of the cumulative value of the Fraction of Absorbed Photosynthetically Active Radiation over the growing season (zCFAPAR) is used as a proxy of seasonal productivity. Results show that the strength of the link varies in space as a function of both the SPI timescale and the timing of the SPI calculation with respect to the vegetative season's progress. For productivity forecasting, we propose an operational strategy to select per grid cell the SPI timescale and computation time with the highest correlation with zCFAPAR at different moments of the season. The linear relationship between SPI and zCFAPAR is significant for 32–66% of the study area, depending on the timing at which SPI is considered (at 0% and 75% of the seasonal progress, respectively). For these areas, the selected SPI explains on average about 40% of the variance of zCFAPAR and may thus assist in the earlier identification of agricultural drought.

ARTICLE HISTORY
Received 21 June 2016
Accepted 8 November 2016

1. Introduction

Drought, with its negative effects on agro-pastoral production, is one of the main causes of food insecurity worldwide. Mitigating drought impacts requires timely and location-specific information on drought occurrence to ensure appropriate responses (Rembold et al. 2016).

Vegetation status can be efficiently monitored at the regional scale in near-real time using satellite data (Brown 2008). This is typically achieved with vegetation indexes or biophysical variables such as the fraction of absorbed photosynthetically active radiation (FAPAR). Despite being useful and objective, such assessments can only be performed when vegetation development has already been affected by drought.

CONTACT Michele Meroni michele.meroni@jrc.ec.europa.eu Directorate D - Sustainable Resources, Food Security Unit, European Commission, Joint Research Centre, Via E. Fermi 2749, Ispra I-21027 VA, Italy

Table 1. Remote sensing-derived data products used. RFE stands for rainfall estimates.

Variable	Source	Resolution		Start year	Reference and web link
		Spatial (km)	Temporal (days)		
RFE	TAMSAT	4	10	1983	Tarnavsky et al. 2014; tamsat.org.uk/cgi-bin/data
RFE	CHIRPS	6	10	1981	Funk et al. 2015; chg.geog.ucsb.edu/data/chirps
FAPAR	JRC	1	10	1999	Weiss et al. 2010; available upon request to authors, most recent algorithm version at land.copernicus.eu/global

Rainfall deficit is the main trigger for agricultural drought, even though other factors such as air temperature, humidity, wind speed, and soil properties also play a role. For this reason, various early warning monitoring systems (e.g., the US Famine Early Warning Systems Network; the Global Information and Early Warning System of the Food and Agriculture Organization) monitor rainfall to anticipate crop and rangeland performance. In this study, we evaluate the performance and timeliness of the Standardized Precipitation Index (SPI, World Meteorological Organization 2012; McKee et al. 1993), an index widely used to characterize meteorological drought at a range of timescales, in anticipating deviations from mean seasonal vegetation productivity in the Sahel. We computed the SPI at various timescales from two sources of satellite-derived rainfall estimates (RFE), that is, the Tropical Applications of Meteorology Using Satellite Data and Ground-Based Observations (TAMSAT), and the Climate Hazards Group Infrared Precipitation with Station (CHIRPS). We calculated a proxy of the seasonal primary productivity by the phenology-based seasonal sum of FAPAR (CFAPAR) obtained from the SPOT (Satellite Pour l'Observation de la Terre) VEGETATION mission (e.g., Meroni, et al. 2014a; Prince 1991). Product characteristics are reported in Table 1. Although retrospective studies investigating the relationship between annual rainfall and vegetation productivity exist (e.g., Fensholt and Rasmussen 2011; Kattelus et al. 2016; Pei et al. 2013), the linkage between anomalies of seasonal productivity and precipitation at various stages of the growing cycle has not been investigated previously.

2. Data and case study description

We investigated the link between RFE-derived SPI and FAPAR-derived anomalies of seasonal productivity for the period 1999–2013 in the Sahel. We limited the analysis to cropland and rangeland areas, according to GLC2000 global land cover at 1 km spatial resolution (Bartholomé and Belward 2005), and to the five main ecoregions of the Sahel (Olson et al. 2001) between 8° and 20°N. Mean annual precipitation increases from 340 mm in the north to 710 mm in the south. A more elaborate description of the study area can be found in Meroni, et al. (2014a). Remotely sensed data used in this study are listed in Table 1.

Although the relationship between rainfall and biomass development is expected to be weakened for irrigated croplands, we did not exclude them from the analysis because reliable mapping of irrigated areas is difficult due to their dynamic character (Thenkabail et al. 2009), while existing land cover data sets show that they constitute only a minor fraction (1.6%) of the total crop area (Vancutsem et al., 2013). Moreover, we found

results to be largely insensitive to the inclusion/exclusion of irrigated land (using Vancutsem et al., 2013) from the analysis (data not shown).

3. Methods

The SPI is a probability index that expresses the observed cumulative precipitation for a given timescale (i.e., the period during which precipitation is accumulated) as the standardized departure from the rainfall probability distribution function. The frequency distribution of historical rainfall data for a given grid cell and timescale is fitted to a gamma distribution and then transformed into a standard normal distribution. It is suggested that a minimum of 30 years of precipitation data should be used to fit the parametric distribution (McKee et al. 1993). To keep the time frame consistent for the two RFE sources, we computed the SPI using data for the 1983–2013 period, using the SPIRITS software (Rembold et al., 2015). Six rainfall accumulation periods, from 1 to 6 months (m), are used to generate SPI_m series for every 10 days during the entire 30-year period. That is, we used an accumulation window of fixed length m and then computed the SPI_m series by moving this window over the time series in 10-day steps. It is noted that the window is not centred but extends backwards in time from each data point. Thus, for instance, SPI_1 for the 10-day period 11–20 February is computed using the rainfall accumulated over the previous month (21 January–20 February).

The proxy of biomass production (CFAPAR) is computed as the cumulative FAPAR value over the average growing season period. This period is defined for each grid cell using the average timing of the start and end of season (SOS, EOS). SOS and EOS were estimated from the FAPAR time series by iterative fitting of a double hyperbolic tangent model per grid cell and per season within the time series as described in Meroni, et al. (2014b) and modifications (Vrieling et al., 2016). Different spatial resolutions are matched by assigning the mean CFAPAR within each cell of the two coarser-resolution SPI sources. Standard scores of the 15-year long time series of CFAPAR are then computed (further referred to as zCFAPAR). Modal resampling was used for the GLC2000 land cover layer. CFAPAR and land cover information were thus rescaled to 4 and 6 km for the analysis with TAMSAT and CHIRPS data, respectively.

To evaluate the potential and timeliness of SPI as an early indicator of seasonal vegetation productivity, we calculated the coefficient of determination (R^2) of the linear regression between zCFAPAR (dependent variable) and the various $SPI_{m,t}$ (independent variables) computed for different accumulation periods (m), and different progress stages of season, denoted by subscript t. Five progress stages, expressed as percentage of the season period, were considered, that is, from the season's beginning (t = 0%, corresponding to SOS) to its end (t = 100%, corresponding to EOS) in incremental steps of 25%. As mentioned above, the SPI_m values are available for the entire time series at a 10-day time step. With the use of t we aim to select, per grid cell, the SPI_m time observation that is available when a percentage t of the growing season has elapsed. For instance, $SPI_{1,25}$ is the SPI value computed with an accumulation period of 1 month and referring to the time of the year for which 25% of the growing season period has completed (i.e., time of year = SOS + 0.25 × (EOS-SOS)). Note that the seasonal progress value corresponds to different times of the year for different grid cells. In summary, for

each grid cell we consider the 30 $SPI_{m,t}$ originating from the combination of six rainfall accumulation periods m and five computation times corresponding to progresses t.

The R^2 was computed independently for each grid cell using 15 data points (i.e., years). To summarize our findings, we first assessed the mean R^2 resulting from the selection of a single optimal $SPI_{m,t}$ for the entire study area. This strategy represents the typical use of SPI in operational monitoring. Tukey's honest significant difference (HSD) test was employed to test significant differences among such R^2 spatial averages over the study area. Then we assessed per grid cell which combination of m and t provided the largest R^2. This assessment can only be applied retrospectively, and is performed here to study the variability of SPI timescales as a function of seasonal progress. Finally, we explored an operational strategy for early warning purposes that selects per grid cell the optimal accumulation period m and observation time, expressed in terms of season progress t.

4. Results and discussion

The R^2 values between zCFAPAR and the various $SPI_{m,t}$ were larger when using CHIRPS in the SPI computation (Table 2). Nevertheless, the ranking of the various SPIs was similar for CHIRPS- and TAMSAT-based SPIs. For conciseness and clarity, the following discussion will focus on CHIRPS-derived indexes only.

4.1. *Selecting a single SPI*

Table 2 shows that the largest mean R^2 (0.22) are found for SPIs computed half-way through the season and with long accumulation periods (4–6 months, thus detecting the more severe droughts). The growing season length varies in the study area between 1–6 months from north to south (for details see Meroni, et al., 2014a). Thus, such SPIs cover roughly the season experienced so far plus an additional preseason period of variable length. Ji and Peters (2003) also found the strongest correlations between SPI and NDVI to occur during the middle of the growing season in the central US Great Plains, but using a shorter accumulation period for SPI (3 months).

For a large fraction of the grid cells (e.g., 63% for $SPI_{6,50}$) there is no significant linear relationship (p-value = 0.05) between the two variables. According to the HSD test, all the $SPI_{m,t}$ denoted by the same letters (e.g., *a* and *ab*) are equally effective (i.e., not significantly different). $SPI_{6,100}$, computed at the EOS, is not ranked among the largest R^2 and belongs to the fourth HSD group (*d*), indicating that rainfall in the final period of the season, when vegetation is in the senescence phase, is less important. This is corroborated by the fact that short SPI timescales (e.g., m = 1 or 2) show the smallest R^2 when computed around the EOS (t = 75% and 100%). Compared to half-way through the season, earlier SPIs (25% progress) show slightly smaller R^2 (0.2) and area covered by a significant regression (31%). At the SOS (0% progress), $SPI_{2,0}$ has the largest R^2 (0.17) and is significantly different from other SPIs. Thus, the rainfall during a relatively short preseason period may contribute to the prediction of seasonal vegetation productivity.

The R^2 for rangelands is in all cases larger than for croplands, which corroborates the findings of Pei et al. (2013) who analysed the spatial correlation of SPI and net primary production during drought years in China. This likely reflects the fact that rangeland

Table 2. Fraction of total number of pixels having a significant regression at p-value = 0.05.

RFE	SPI accumulation period, m (months)	Progress of the season, t (%)	Fraction with significant regression (p = 0.05) (%)	R^2 Overall Avg	SD	Min	Max	HSD group	Cropland AVG	Rangeland AVG
CHIRPS	6	50	36.60	0.221	0.17	0.00	0.88	a	0.197	0.249
	5	50	36.55	0.221	0.17	0.00	0.88	ab	0.197	0.249
	4	50	36.32	0.220	0.17	0.00	0.87	ab	0.195	0.249
	6	75	36.35	0.219	0.17	0.00	0.89	b	0.198	0.242
	5	75	35.46	0.215	0.17	0.00	0.89	c	0.192	0.241
	6	100	34.48	0.210	0.17	0.00	0.85	d	0.186	0.237
	3	50	33.10	0.207	0.17	0.00	0.90	e	0.174	0.244
	4	75	32.30	0.201	0.16	0.00	0.88	f	0.171	0.235
	5	100	31.59	0.198	0.16	0.00	0.88	g	0.168	0.231
	3	25	30.83	0.197	0.17	0.00	0.87	g	0.180	0.217
	6	25	30.78	0.197	0.17	0.00	0.88	g	0.181	0.215
	4	25	30.80	0.197	0.17	0.00	0.88	g	0.180	0.215
	5	25	30.76	0.196	0.17	0.00	0.88	g	0.180	0.215
	2	25	27.90	0.185	0.16	0.00	0.90	h	0.160	0.212
	4	100	28.20	0.183	0.16	0.00	0.85	h	0.149	0.222
	3	75	27.68	0.181	0.16	0.00	0.87	i	0.145	0.220
	2	50	25.64	0.173	0.15	0.00	0.86	j	0.137	0.214
	2	0	24.54	0.169	0.15	0.00	0.86	k	0.151	0.188
	6	0	23.81	0.165	0.15	0.00	0.89	l	0.150	0.182
	5	0	23.78	0.165	0.15	0.00	0.89	l	0.150	0.182
	4	0	23.77	0.165	0.15	0.00	0.89	l	0.149	0.182
	3	0	23.80	0.165	0.15	0.00	0.90	l	0.150	0.182
	1	0	23.31	0.162	0.15	0.00	0.89	m	0.150	0.175
	3	100	20.36	0.149	0.14	0.00	0.86	n	0.114	0.189
	2	75	19.25	0.144	0.14	0.00	0.86	o	0.114	0.177
	1	25	17.63	0.135	0.14	0.00	0.87	p	0.111	0.163
	1	50	14.94	0.127	0.13	0.00	0.83	q	0.108	0.148
	2	100	12.24	0.109	0.12	0.00	0.88	r	0.093	0.127
	1	75	10.07	0.096	0.11	0.00	0.84	s	0.083	0.110
	1	100	5.49	0.074	0.09	0.00	0.86	t	0.069	0.077
TAMSAT	4	50	29.58	0.190	0.17	0.00	0.93	a	0.166	0.218
	6	75	28.83	0.189	0.17	0.00	0.88	ab	0.171	0.209
	6	50	28.92	0.188	0.17	0.00	0.93	b	0.163	0.216
	5	50	28.90	0.188	0.17	0.00	0.93	b	0.164	0.215

Average (Avg) and standard deviation (SD) of R^2 between $SPI_{m,t}$ and zCFAPAR for the entire study area (overall), croplands and rangelands. SPI indicators are listed in descending order of average R^2. Significant differences among means are denoted by different letters (Tukey's HSD test, p = 0.05). Only the first two HSD groups are reported for TAMSAT (with separate grouping from CHIRPS).

productivity has a stronger direct dependency on rainfall, while cropland productivity is strongly affected by management practices such as ploughing, weeding, and irrigation.

4.2. *Selecting SPI at the grid cell level*

The mean R^2 over the study area is larger if m and t are selected at the grid cell level. In such conditions, the mean overall R^2 is 0.36 (0.34 and 0.37 for croplands and rangelands, respectively). Figure 1 shows the spatial distribution of m and t that provides the largest R^2. The fraction of grid cells with a statistically significant linear regression (p-value = 0.05) is 68%. Large spatial variability in R^2, as well as in optimal SPI timescale and time of computation, is present in the study area, similar to results of Kattelus et al. (2016) studying the correlation of SPI and rice yield in South Asia.

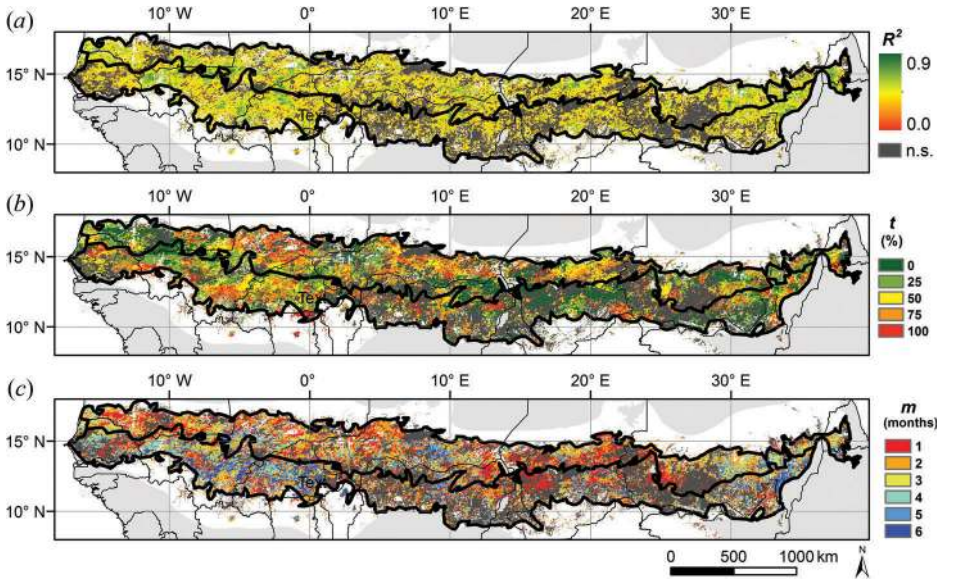

Figure 1. (*a*): Coefficient of determination of the linear regression between zCFAPAR and SPI *m.t, m* and *t* are selected at the pixel level as the pair providing the largest R^2 value. n.s. stands for not significant at *p*-value = 0.05. (*b*) and (*c*): progress of the season (*t*) and accumulation period (*m*) of the selected SPI. Data shown for rangeland and cropland land cover (other classes in white) and the five main ecoregions of the Sahel (other areas in grey). The thick black simplified polygons represent the rangeland (in the North) and cropland (in the South) bands.

Table 3. Percentage of pixels selected (over the total pixels with a significant relationship) by progress of the season and SPI accumulation period as a result of the maximum R^2 selection of Figure 2. Min. (white)–max. (green) colour coding is applied to percentages.

	Progress of the season, *t* (%)					
SPI accumulation period, *m* (months)	0	25	50	75	100	Row total
1	12	5	5	5	2	28
2	6	6	4	4	4	24
3	3	4	4	3	3	17
4	2	2	4	2	3	13
5	1	2	3	2	1	9
6	0	1	3	3	2	9
Column total	24	20	22	19	15	

Table 3 shows that, in the majority of the cases (69%), the largest R^2 is found when using an accumulation period of 1–3 months. For 66% of the grid cells, the strongest linear link is found during the first half of the season (0–50% progress).

4.3. *Selecting SPI at the grid cell level by time of analysis*

In our last analysis we are interested in determining, when the progress of the grid cell varies from 0% to 100%, what is, on average, the R^2 achievable using the best SPI indicator available. This explores the potential of an operational use of SPI as an early indicator of seasonal vegetation productivity. Each grid cell is characterized by its own

Table 4. Statistics of linear regression $SPI_{m,t}$ vs. zCFAPAR obtained by selecting for each actual seasonal progress T, the accumulation period m and the optimal timing of SPI computation t ($t \le T$) that maximize the R^2.

	Actual progress of the season, T (%)				
	0	25	50	75	100
Average R^2					
Overall	0.20	0.28	0.32	0.35	0.36
Cropland	0.19	0.26	0.31	0.33	0.34
Rangeland	0.22	0.30	0.34	0.36	0.37
Fraction of pixels with significant regression (p = 0.05)					
	32.09	49.22	60.18	65.57	68.18
Average R^2 for pixels with significant regression (p = 0.05)					
	0.40	0.42	0.43	0.44	0.44
Percentage of pixels selected by SPI accumulation period					
1 month	46	34	30	29	28
2 months	27	27	24	23	24
3 months	12	18	17	17	17
4 months	11	12	15	12	13
5 months	3	7	8	9	9
6 months	2	3	6	9	9
Percentage of pixels selected by time of SPI computation time					
t = 0%	100	42	29	25	24
t = 25%	–	58	27	22	20
t = 50%	–	–	44	25	22
t = 75%	–	–	–	28	19
t = 100%	–	–	–	–	15

For each actual progress of the season, the percentage of pixels by the selected SPI accumulation period and by the time of SPI computation is shown with min. (white)–max. (green) colour coding.

phenology and, at a given time during which the analysis is performed, by its specific progress of the season. We further refer to this cell-specific actual progress of the season at the time of analysis as capital T. Per grid cell, we thus select the SPI accumulation period (m) and its available progress stage t (with $t \le T$) that provides the largest R^2 in explaining zCFAPAR at the actual (and current) progress stage T. Clearly, not all m,t-combinations are available when the vegetative season progress has not yet reached the 100% progress for a given grid cell. For instance, if T = 50% for a given grid cell, only SPI computed at t = 0%, 25% and 50% can be calculated. We note that results gathered at the end of the season (T = 100%) would give the same results as the one presented in detail in the previous section. Statistics of the linear regression between CFAPAR and the various SPIs computed at each step of the seasonal progress are reported in Table 4.

For the same actual progress of the season, the average R^2 and the fraction of grid cells having a statistically significant regression presented in Table 4 (grid cell-based selection of the accumulation period and timing of SPI computation) is greater than that in Table 2, which refers to a unique accumulation period for all grid cells.

At the beginning of the season (T = 0%), we observe a significant linear relationship for about one-third of the grid cells. For such grid cells, the average R^2 is 0.4 and the shortest accumulation periods are used for SPI computation. Thus, when using SPI as a predictor of the coming growing season, we should mask out regions with non-significant relationships, and we should be aware that the variance of zCFAPAR explained by SPI is limited to 40%.

When the actual season progresses up to 25% and 50% the fraction of the area showing a significant relationship increases (to 49% and 60%, respectively), and longer

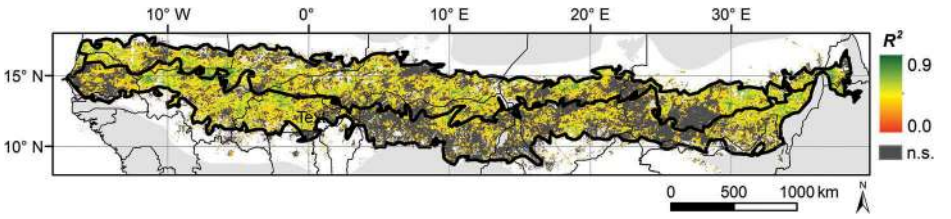

Figure 2. Coefficient of determination of the linear regression between zCFAPAR and $SPI_{m,t}$ that can be computed half-way through the season (T = 50%) by selecting best accumulation period m and timing for SPI computation t. n.s. stands for not significant at p-value = 0.05.

SPI accumulation periods are selected (Table 4). Figure 2 shows the R^2 spatial patterns for 50% progress of the season.

5. Comparison of SPI selection methods

The limits to the usability of SPI to provide information about seasonal vegetation productivity were identified by selecting, for each location, the best combination of accumulation period and progress of the season for computing SPI (mean overall spatial R^2 = 0.36). Obviously, a method that selects each optimal stage of seasonal progress for calculating the SPI cannot be used for operational drought prediction within the season as it requires the full seasonal information. At the same time, we found that the traditional use of SPI as a drought indicator, that is, the selection of a single period for the SPI computation regardless location and seasonal progress, is not the most effective approach for the purpose (best R^2 ranging from 0.17 to 0.22 depending on season progress). We showed that a better operational strategy is a per-grid cell selection of the most appropriate accumulation period (m) and timing of SPI computation (t) for the actual seasonal progress (T) (R^2 = 0.20– 0.37 depending upon progress). Due to the time lag between rainfall and vegetation response, SPIs computed at early season stages can still be selected when performing the analysis at later stages. For instance, at 75% actual seasonal progress, SPIs computed for earlier stages (from 0% to 50%) are selected for 72% of the grid cells.

Several factors may play a role in weakening the link between the meteorological drought indicator (SPI) and the agricultural drought indicator (zCFAPAR). First, a confounding factor may be the uncertainty in RFE affecting the accuracy of the drought indicator (Naumann et al. 2014). Second, reduced functional dependence is expected in areas where precipitation is not a strong limiting factor or in areas with little inter-annual variability of precipitation. In fact, the strength of such dependence (R^2 of $SPI_{6,50}$ as an example) is significantly and negatively correlated with the mean annual precipitation (correlation coefficient r = −0.26), while positively and significantly correlated with the coefficient of variation of the annual precipitation (r = 0.26). Third, deviation from a linear relation is expected in areas where the amount of water that is available to plants differs substantially from cumulative rainfall because of processes such as direct evaporation and water run-off/on. Hence, improving the relationship of precipitation with zCFAPAR may require modelling the soil-available water using soil water balance models (e.g., Frere and Popov 1986). Fourth, a

precipitation feature that is not captured in SPI, the temporal rainfall distribution, is also expected to add noise as the same amount of cumulative rainfall may result in different production levels depending on their temporal distribution (Hiernaux et al. 2009). For example, uniformly distributed rainfall across the season will result in less vegetation stress compared with heavy rainfall events separated by dry intervals (Zhang et al. 2013). Finally, areas subjected to flooding may present an inverse relationship.

6. Conclusions

This study shows that the most effective approach for using SPI as an operational early indicator of vegetation productivity anomalies is to consider vegetation phenology and select the SPI accumulation period and time of computation separately for each grid cell at each time of analysis.

Disclosure statement

No potential conflict of interest was reported by the authors.

References

Bartholomé, E. M., and A. S. Belward. 2005. "GLC2000: A Newapproach to Global Land Cover Mapping from Earth Observation Data." *International Journal of Remote Sensing* 26: 1959–1977. doi:10.1080/01431160412331291297.

Brown, M. E. 2008. *Famine Early Warning Ststems and Remote Sensing Data*. Berlin Hidelberg: Springer-Verlag. doi:10.1017/CBO9781107415324.004.

Frere, M., and G. F. Popov. 1986. Early agrometeorological crop yield assessment. FAO Plant Production and Protection paper No. 17. FAO, Rome.

Fensholt, R., and K. Rasmussen. 2011. "Analysis of Trends in the Sahelian 'Rain-Use Efficiency' Using GIMMS NDVI, RFE and GPCP Rainfall Data." *Remote Sensing of Environment* 115: 438–451. doi:10.1016/j.rse.2010.09.014.

Funk, C., P. Peterson, M. Landsfeld, D. Pedreros, J. Verdin, S. Shukla, G. Husak, J. Rowland, L. Harrison, A. Hoell, and J. Michaelsen. 2015. "The Climate Hazards Infrared Precipitation With Stations—a New Environmental Record For Monitoring Extremes." *Scientific Data* 2, 150066. doi:10.1038/sdata.2015.66

Hiernaux, P., E. Mougin, L. Diarra, N. Soumaguel, F. Lavenu, Y. Tracol, and M. Diawara. 2009. "Sahelian Rangeland Response to Changes in Rainfall over Two Decades in the Gourma Region, Mali." *Journal of Hydrology* 375: 114–127. doi:10.1016/j.jhydrol.2008.11.005.

Ji, L., and A. J. Peters. 2003. "Assessing Vegetation Response to Drought in the Northern Great Plains Using Vegetation and Drought Indices." *Remote Sensing of Environment* 87: 85–98. doi:10.1016/S0034-4257(03)00174-3.

Kattelus, M., A. Salmivaara, I. Mellin, O. Varis, and M. Kummu. 2016. "An Evaluation of the Standardized Precipitation Index for Assessing Inter-Annual Rice Yield Variability in the Ganges-Brahmaputra-Meghna Region." *International Journal of Climatology* 36: 2210–2222. doi:10.1002/joc.4489.

McKee, T. B., N. J. Doesken, and J. Kleist, 1993: "The Relationship Of Drought Frequency And Duration To Time Scale." In *Proceedings of the Eighth Conference on Applied Climatology*, Anaheim, California,17–22 January 1993. Boston, American Meteorological Society, 179–184

Meroni, M., F. Rembold, M. M. Verstraete, R. Gommes, A. Schucknecht, and G. Beye. 2014a. "Investigating the Relationship between the Inter-Annual Variability of Satellite-Derived

Vegetation Phenology and a Proxy of Biomass Production in the Sahel." *Remote Sensing* 6: 5868–5884. doi:10.3390/rs6065868.

Meroni, M., M. M. Verstraete, F. Rembold, F. Urbano, and F. Kayitakire. 2014b. "A Phenology-Based Method to Derive Biomass Production Anomalies for Food Security Monitoring in the Horn of Africa." *International Journal of Remote Sensing* 35: 2472–2492. doi:10.1080/01431161.2014.883090.

Naumann, G., E. Dutra, P. Barbosa, F. Pappenberger, F. Wetterhall, and J. V. Vogt. 2014. "Comparison of Drought Indicators Derived from Multiple Data Sets over Africa." *Hydrology and Earth System Sciences* 18: 1625–1640. doi:10.5194/hess-18-1625-2014.

Olson, D. M., E. Dinerstein, E. D. Wikramanayake, N. D. Burgess, G. V. N. Powell, E. C. Underwood, J. A. D'amico, et al. 2001. "Terrestrial Ecoregions of the World: A New Map of Life on Earth." *BioScience* 51: 933. doi:10.1641/0006-3568(2001)051[0933:TEOTWA]2.0.CO;2.

Pei, F., X. Li, X. Liu, and C. Lao. 2013. "Assessing the Impacts of Droughts on Net Primary Productivity in China." *Journal of Environmental Management* 114: 362–371. doi:10.1016/j.jenvman.2012.10.031.

Prince, S. D. 1991. "Satellite Remote Sensing of Primary Production: Comparison of Results for Sahelian Grasslands 1981-1988." *International Journal of Remote Sensing* 12: 1301–1311. doi:10.1080/01431169108929727.

Rembold, F., M. Meroni, C. Atzberger, F. Ham, and E. Fillol. 2016. "Agricultural Drought Monitoring Using Space-Derived Vegetation and Biophysical Products: A Global Perspective." In *Remote Sensing Handbook, Volume III: Remote Sensing of Water Resources, Disasters and Urban Studies*, edited by P. S. Thenkabail, 349–365. Boca Raton, FL: CRC Press.

Rembold, F., M. Meroni, F. Urbano, A. Royer, C. Atzberger, G. Lemoine, H. Eerens, and D. Haesen. 2015. "Remote Sensing Time Series Analysis for Crop Monitoring with the SPIRITS Software: New Functionalities and Use Examples." *Frontiers in Environmental Science* 3: 129–134. doi:10.3389/fenvs.2015.00046.

Tarnavsky, E., D. Grimes, R. Maidment, E. Black, R. P. Allan, M. Stringer, R. Chadwick, and F. Kayitakire. 2014. "Extension of the TAMSAT Satellite-Based Rainfall Monitoring over Africa and from 1983 to Present." *Journal Of Applied Meteorology And Climatology* 53: 2805–2822. doi:10.1175/JAMC-D-14-0016.1

Thenkabail, P. S., C. M. Biradar, P. Noojipady, V. Dheeravath, Y. Li, M. Velpuri, M. Gumma, et al. 2009. "Global Irrigated Area Map (GIAM), Derived from Remote Sensing, for the End of the Last Millennium." *International Journal of Remote Sensing* 30: 3679–3733. doi:10.1080/01431160802698919.

Vancutsem, C., E. Marinho, F. Kayitakire, L. See, and S. Fritz. 2013. "Harmonizing and Combining Existing Land Cover/Land Use Datasets for Cropland Area Monitoring at the African Continental Scale." *Remote Sensing* 5: 19–41. doi:10.3390/rs5010019.

Vrieling, A., M. Meroni, A. G. Mude, S. Chantarat, C. C. Ummenhofer, and K. De Bie. 2016. "Early Assessment of Seasonal Forage Availability for Mitigating the Impact of Drought on East African Pastoralists." *Remote Sensing of Environment* 174: 44–55. doi:10.1016/j.rse.2015.12.003.

Weiss, M., F. Baret, H. Eerens, and E. Swinnen. 2010. "FAPAR over Europe for the Past 29 Years: A Temporally Consistent Product Derived from AVHRR and VEGETATION Sensors." In *Proceedings of the Third RAQRS Workshop*, Valencia, Spain, 27 September–1 October 2010, 428–433.

World Meteorological Organization. 2012. *Standardized Precipitation Index User Guide*. Geneva: World Meteorological Organization.

Zhang, Y., M. S. Moran, M. A. Nearing, G. E. P. Campos, A. R. Huete, A. R. Buda, D. D. Bosch, et al. 2013. "Extreme Precipitation Patterns and Reductions of Terrestrial Ecosystem Production across Biomes." *Journal of Geophysical Research: Biogeosciences* 118 (1): 148–157. doi:10.1029/2012JG002136.